

Contribution to the CCP-WSI Blind Test Series 3: Analysis of scaling effects of moored point-absorber wave energy converters in a CFD-based numerical wave tank

Christian Windt and John V. Ringwood

Centre for Ocean Energy Research, Maynooth University, Co. Kildare, Ireland

Josh Davidson

Department of Fluid Mechanics, Faculty of Mechanical Engineering, Budapest University of Technology and Economics, Hungary

Pál Schmitt

Marine Research Group, Queen's University Belfast, Northern Ireland

ABSTRACT

Computational fluid dynamics (CFD) based numerical wave tanks (NWTs) can provide valuable insight into the hydrodynamic performance of wave energy converters (WECs). Being able to capture hydrodynamic non-linearities, CFD-based NWTs (CNWTs) allow the analysis of WECs over a wide range of test conditions, such as sea states, power take-off control settings and model scale. The capabilities of a CNWT are exploited in this paper, which aims to analyse of the scaling effects of two moored point-absorber type WECs, exposed to focussed waves. To this end, three different scales are considered: 1:1, 1:10 and 1:10_{PWT}. The latter, 1:10_{PWT} scale, refers to the typical scale used in physical wave tanks (PWTs), complying with Froude scaling, but violating Reynolds scaling. In the 1:10 scale model, fluid viscosity is scaled, in line with the geometric properties, thereby achieving both Froude and Reynolds similitude. From the results, average differences between the three considered scales of around 5% have been observed, and the overall greatest sensitivity to scale effects can be found in the surge and pitch degree of freedom.

KEY WORDS: Wave Energy, CCP-WSI Blind Test, Impulse wave maker, CFD, numerical wave tank, OpenFOAM, Scaling

INTRODUCTION

In recent years, the public awareness and recognition of global warming has fuelled the research and development (R&D) of novel technologies to harness renewable energy resources. Amongst these resources, marine renewable energies, and specifically ocean wave energy, show significant potential to contribute to the global energy supply (de O. Falcão, 2010). The harsh ocean environment, in which WECs are deployed, poses challenges to the R&D of these devices. Although the energy resource is available at no cost, to be commercially viable, the cost of the produced energy from a WEC has to be minimised, following the premiss of converting maximum energy at minimal cost. The evaluation of the cost

of energy, commonly referred to as Levelised Cost of Energy (LCoE), includes expenditures for device manufacturing, deployment, operation, maintenance and decommissioning. The operational costs are e.g. driven by the structural loads on the devices in power production mode, as well as in extreme cases, which are considerable, since WECs will typically be located at sites exposed to powerful wave climates.

Scale model testing

To design an efficient, economical and survivable WEC, engineers mostly rely on physical and numerical model testing. During physical testing, WECs are commonly modelled at small scale, applying the Froude scaling law to scale dimensions of the structure and wave characteristics. However, fluid viscosity can not be correctly scaled in PWTs. This leads to the well known discrepancy between Froude and Reynolds scaling, which undermines the confidence in up-scaled results from PWT tests (Veritas, 2000). The only way to overcome this issue during physical testing would be through full scale testing or testing with a fluid of lower viscosity, requiring extensive capital expenditure. O'Boyle et al. (2015) provide one of the few comparisons of full scale results to scaled experimental tests, highlighting issues related to accuracy and resolution of off-shore instrumentation.

A powerful feature of CNWTs is the ability to easily change the scale of the considered WEC, at virtually zero cost, compared to PWTs. Within the CNWT, both structural dimensions and wave conditions, as well as the fluid viscosity, can easily be scaled. Thereby, CNWTs provide a tool to assess the error, related to scaling effects in PWTs.

Related studies

In the literature, a number of studies can be found, investigating the effect of different scales during model testing. Wei et al. (2013, 2015) investigate scaling effects on an oscillating wave surge converter (OWSC), for cases of an undamped, damped and fixed flap, in regular waves. Negligible differences are found for scales between 1:1 and 1:100. Deviations between the scales were only observed when analysing the vorticity

ity; however, the overall effect of these deviations is diminished by scale independent effects. It should be noted that the wall treatment has not been adjusted for the different scales, undermining the numerical results. Also considering an OWSC, Schmitt and Elsässer (2017) investigate the application of Froude scaling by changing the viscosity of the fluid in the CNWT, while retaining the dimensions of the structure and the tank. As expected and confirmed by field data, the formation of bubbles at full scale is observed in the numerical model. Comparing rotation angles and power output, small deviations of $\leq 5\%$ are found. The authors also point out the importance of the correct wall treatment and requirements on meshes for different scales.

Mundon et al. (2017) perform drag identification tests at various model scales, and find validity of the scaling laws for high Keulegan-Carpenter (KC) and low Reynolds numbers. For lower KC numbers, the scaling rules fail, leading to overestimation of the drag coefficients.

Investigating oscillating water columns (OWCs), Elhanafi et al. (2017) study the influence of model scale and air compressibility on the WEC efficiency. With the assumption of incompressible air, the scaling effects are negligible; however, analysis at full scale including compressible air shows a considerable reduction in the efficiency.

Most recently, Palm et al. (2018) assess the effects of scale, viscous forces and induced drag on a moored point-absorber WEC. For that, simulations at full scale, as well as 1:16 model scale are performed. Using Reynolds-Averaged Navier Stokes (RANS), Euler and linear radiation-diffraction simulation methods, the authors were able to break down the effect of non-linear mooring response, Froude-Krylov and viscous forces, as well as induced drag, non-linear added mass and radiation forces on the device dynamics. Concluding, the authors suggest the use of experimental tank test, together with RANS and Euler simulations, to gain a complete understanding of scale-dependent and -independent effects.

Current study

While Schmitt and Elsässer (2017) only consider scaling of the fluid viscosity and Palm et al. (2018) consider scaling of the geometric dimensions, this study considers scaling both the fluid viscosity and geometric dimensions, as well as scaling geometric dimensions only, to analyse the effect of different model scales. The case of scaled geometrical dimensions with full scale fluid viscosity represents the typical model setup in a PTW. Hence, this study allows the analysis of the *scaling error* in PWTs.

CCP-WSI Blind Test

The structures under investigation are the two moored point-absorber WECs considered in the *Collaborative Computational Project in Wave Structure Interaction (CCP-WSI) Blind Test Series 3* (see CCP-WSI Blind Test Series 3 website (2018)). WEC 1 (W1) is a hemispherical bottom buoy (see Fig. 1a); WEC 2 (W2) is a cylindrical buoy with a moon-pool (see Fig. 1b). The structures are exposed to three different focussed waves.

For the blind test, PWT tests are performed, and relevant measurements of free surface elevation (FSE), device motion and mooring force are acquired. Participants of the blind tests are then provided with the physical properties of the tank test (tank dimensions, measurement location, body mass, etc.), in order to perform the simulation with their CNWT setup. The numerical results of the FSE, device motion and mooring force are submitted for a blind comparison with the experimental reference. The results presented in this paper, for the small scale model simulation with geometric scaling, are submitted to this blind test competition.

Outline of paper

The remainder of this paper is organised as follows: Section 2 provides a brief overview of the scaling laws applied in this study. Section 3

(a) WEC 1 (W1)



(b) WEC 2 (W2)



Fig. 1 WEC 1 (W1) is a hemispherical bottom buoy; WEC 2 (W2) is a cylindrical buoy with a moon-pool.

presents the details of the experimental setup and test cases. Following that, Section 4 describes the setup of the CNWT used throughout this study. In Section 5, the results for the three different waves are presented and discussed. Finally conclusions are drawn in Section 6.

SCALING

For the scaling of the relevant physical properties, the Froude scaling law is applied throughout this study. The physical parameters are simply scaled by multiplication of the corresponding quantity with the linear scaling factor, listed in Table 1. For the case at hand, the length scale factor is $\sigma = 1/10$.

As mentioned in Section 1, special attention must be paid to the scaling of the fluid viscosity ν . In PWTs, viscosity can not be scaled easily whereas, in CNWTs, the required adjustment can be made simply by changing a parameter value in the code. Based on the units of ν , i.e. $[\text{m}^2 \text{s}^{-1}]$, and the scaling factors given in Table 1, the viscosity should be scaled as:

$$\nu_{MS} = \nu_{FS} \cdot \frac{\sigma^2}{\sqrt{\sigma}}, \quad (1)$$

where the subscript *MS* refers to model scale and *FS* refers to full scale. In this study, two different scales, i.e. 1:1 (*FS*) and 1:10 (*MS*), are analysed. Furthermore, at 1:10 scale, two cases are considered, representing

1) Froude and Reynolds scaling, i.e. scaling geometric properties, mass, forces, inertial properties, as well as fluid viscosity. This case is henceforth referred to as 1:10

2) Only Froude scaling, i.e. scaling geometric properties, such as mass, forces, and inertial properties, but using full scale fluid viscosity. Since this case mimics the scaling applied in PWTs, it is henceforth referred to as 1:10_{PWT}

Table 1 Froud scaling factors

Physical parameter	Unit	Scaling factor
Length	[m]	σ
Mass	[kg]	σ^3
Force	[N]	σ^3
Torque	[Nm]	σ^4
Acceleration	$[\text{m s}^{-2}]$	1
Time	[s]	$\sqrt{\sigma}$
Pressure	[Pa]	σ

CASE STUDY

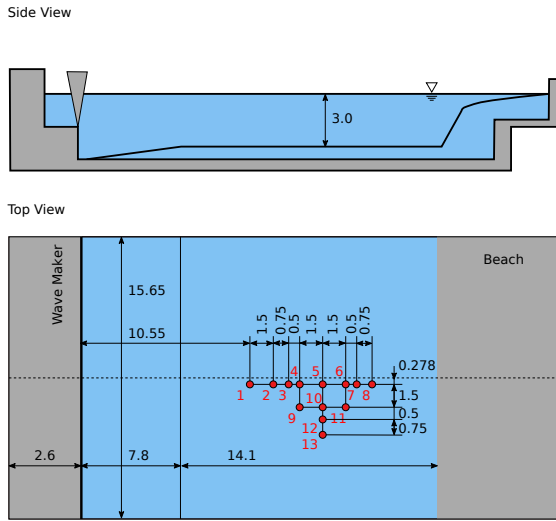
The case study herein is based on CCP-WSI Blind Test Series 3. For the test series, experiments were conducted in the the ocean basin of the COAST laboratory at Plymouth University, specifically for the purpose of CNWT validation. The test campaign includes wave-structure interaction (WSI), as well as wave-only experiments. While the results of the

wave-only experiments are provided to the blind test participants, results of the WSI experiments are, at the time of writing, undisclosed.

Physical wave tank

A schematic of the PWT, with all relevant dimensions, and the wave probe (WP) locations marked in red, is depicted in Fig. 2. A flap-type wave maker is located at the left hand side of the tank. At the right hand side, an absorbing beach is installed, at a distance of 21.9m to the wave maker. The water depth in the test section is set to 3m.

The structures are located at a distance of 14.8m to the wave paddle and 0.278m off the centre line, which coincides with the location of WP 5 in Fig. 2. In total, 13 WPs are distributed in the PWT for the wave-only experiments. For the WSI experiments, WP 5 has been taken out.



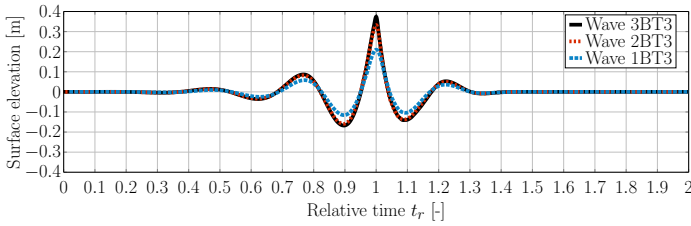


Fig. 4 Experimentally measured 1:10 scale FSE of waves 1BT3–3BT3, at the focal location. The time traces are artificially aligned to match the peaks at $t_r = 1$.

respectively. Here, t denotes time, \mathbf{u} is the fluid velocity, p the fluid pressure, ρ the fluid density, \mathbf{T} the stress tensor and \mathbf{f}_b the external forces such as gravity. In the literature, RANS models, compared to e.g. large eddy simulation models, have proven to be the current industry standard for the modelling of WECs (Windt et al., 2018), avoiding high computational demand. The water wave advection is captured via the Volume of Fluid (VoF) method, proposed by Hirt and Nichols (1981), following

$$\frac{\partial \alpha}{\partial t} + \nabla \cdot (\mathbf{U}\alpha) + \nabla \cdot [\mathbf{U}_r \alpha (1 - \alpha)] = 0 \quad (4)$$

$$\Phi = \alpha \Phi_{\text{water}} + (1 - \alpha) \Phi_{\text{air}} \quad (5)$$

where α denotes the volume fraction of water, \mathbf{U}_r is the compression velocity (Berberović et al., 2009), and Φ is a specific fluid quantity.

The body motion, induced by the incident wave, is solved via Newton's 2nd law of motion within the *sixDoFRigidBodyMotionSolver*, implemented in the OpenFOAM framework. The motion solver provides a set of motion restraints, allowing the implementation of a linear spring to account for the mooring of the device.

To measure the FSE, the iso-surface of the volume fraction $\alpha = 0.5$ is recorded throughout the course of the simulation. The FSE at specific locations, which follow the layout of the PWT (see Fig. 2), can be extracted from the iso-surface data in a post-processing step.

Numerical wave generation and absorption

Different numerical wave makers are available to generate and absorb waves in a CNWT (Windt et al., 2019b). Herein, the impulse source method, proposed by Schmitt et al. (2019), is employed. For this wave maker, a source term, $\mathbf{r}\rho\mathbf{a}_{wm}$, is added to the RANS momentum equation (3), yielding:

$$\frac{\partial \rho \mathbf{U}}{\partial t} + \nabla \cdot \rho \mathbf{U} \mathbf{U} = -\nabla p + \nabla \cdot \mathbf{T} + \rho \mathbf{f}_b + \mathbf{r}\rho\mathbf{a}_{wm} \quad (6)$$

The location of the wave maker zone is defined by $\mathbf{r} = 1$, with $\mathbf{r} = 0$ everywhere else in the domain. \mathbf{a}_{wm} is the field variable acting as acceleration input to the wave maker, which can be determined analytically (Choi and Yoon, 2009) or, as applied here, via an iterative calibration (Schmitt et al., 2019).

For wave absorption, a numerical beach, proposed by Schmitt and Elsaesser (2015), is implemented. Introducing the additional dissipation term, $\mathbf{S}\rho\mathbf{U}$, to the RANS momentum equation (3), yields:

$$\frac{\partial \rho \mathbf{U}}{\partial t} + \nabla \cdot \rho \mathbf{U} \mathbf{U} = -\nabla p + \nabla \cdot \mathbf{T} + \rho \mathbf{f}_b + \mathbf{S}\rho\mathbf{U} \quad (7)$$

The variable field \mathbf{S} controls the strength of the dissipation, with a value of zero in the simulation zone, and then gradually increasing towards the boundary, over the length of the numerical beach, following a pre-defined analytical expression (Schmitt and Elsaesser, 2015).

To control the absorption quality of the numerical beach, the length and the maximum damping factor, \mathbf{S}_{max} , can be adjusted by the user. Based

on the findings of Windt et al. (2019a,b), the length of the numerical beach is set to $1\lambda_{1BT3}$, while the maximum damping factor varies for the different focussed waves. For 1BT3, $\mathbf{S}_{\text{max}} = 5\text{s}^{-1}$ delivers a reflection coefficient³, R , of $\leq 1\%$. For 2BT3 and 3BT3, \mathbf{S}_{max} is increased to 7s^{-1} to maintain the small reflection coefficient. Based on the units of \mathbf{S} , i.e. $[\text{s}^{-1}]$, Froude scaling can be applied for the 1:1 scale case.

A screen-shot of the CNWT, showing the field variable \mathbf{S} , is depicted in Fig. 5a. Screen-shots of the top and side view of the CNWT, showing the field variable α and \mathbf{r} , are shown in Fig. 5b.

Note that the symmetry of the problem is exploited and only half of the PWT is modelled numerically. A symmetry boundary condition is employed in the x,z -plane, where x points in the wave propagation direction, and $-z$ towards the tank floor. This symmetry condition introduces constraints on the body motion, only allowing motion in three degrees of freedom (DoFs), i.e. heave, surge and pitch.

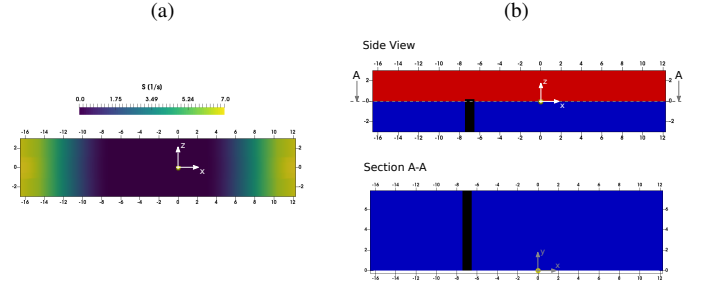


Fig. 5 2D screen-shots of the 1:10 scale CNWT showing the gradually increasing damping factor \mathbf{S} of the numerical beach (a) and the water and air phase (blue and red colour code, respectively) and the impulse source (black colour code) (b). The WEC structure (yellow colour code) is located at $(x, y, z) = (0, 0, 0)$.

Problem discretisation

Convergence studies on the spatial and temporal problem discretisation have been performed, using three different discretisation levels, and are presented in (Windt et al., 2019a). The minimum cell size in the interface region, and around the WEC structure, is 10 cells per significant wave height for wave 1BT3. The maximum aspect ratio in the interface region is 2. Three refinement levels are used to reach the cell size in the interface region. The total cell count for the CNWT at 1:10_{PWT} (and 1:1) scale is 949,584 for G2 and 949,338 for G1. For the CNWT at 1:10 scale, the overall cell count is 1,009,682 for G2 and 962,250 for G1. In temporal terms, a fixed time step size of 0.002s is used. For more details, the interested reader is referred to Windt et al. (2019a).

Viscosity

To achieve Froude and Reynolds scaling in the 1:10 scale case, the fluid viscosity has to be scaled, using the relationship shown in Eq. (1). For the 1:10_{PWT} scale, fluid viscosities of the 1:1 scale case are used. Table 4 lists the different fluid viscosities, of water and air, for all scales.

Turbulence modelling

For the contribution to the CCP-WSI Blind Test Series 2, Windt et al. (2019a) performed an analysis on the necessity of including turbulence modelling, using a standard $k-\omega$ SST turbulence model (Menter, 1992).

³The reflection coefficient is determined using the three point method proposed by Mansard and Funke (1980)

Table 4 Kinematic fluid viscosities for the considered model scales

Scale	Water viscosity [m ² s ⁻¹]	Air viscosity [m ² s ⁻¹]
1:1	1E-6	1.48E-5
1:10 _{PWT}	1E-6	1.48E-5
1:10	3.16E-8	4.68E-7

The considered model scale is 1:10_{PWT}. It was shown that a difference of 5% can be found between simulations including and excluding turbulence modelling. However, given the uncertain validity of the applied wall function, together with the increased run times, laminar conditions are used to determine the final results by Windt et al. (2019a).

Based on the results of Windt et al. (2019a), it is herein assumed that laminar flow conditions hold for the 1:1 model scale, since system dynamics are generally slower in full scale, while the viscosity between the 1:1 and 1:10_{PWT} scale is identical. However, for the 1:10 scale model, turbulent effects may become significant, due to the reduced fluid viscosity. To assess the necessity of turbulence modelling at 1:10 scale, simulations have been run assuming both laminar and turbulent flow conditions⁴. Here, the standard $k-\omega$ SST turbulence model, with industry standard, high Re number, wall functions, is employed. For brevity, the governing equations of the $k-\omega$ SST turbulence model are not presented here, instead the interested reader is referred to Menter (1992). The choice of the turbulence model is based on the literature review presented by Windt et al. (2018), in which the $k-\omega$ SST turbulence model is identified as one of the most commonly used turbulence models in the field of ocean wave energy. A comparison of the different available turbulence models is beyond the scope of the current paper.

Table 5 shows the results for the comparison between turbulent and laminar flow conditions. The largest differences between laminar and turbulent results can be observed for the surge and pitch DoF, which is consistent with (Windt et al., 2019a). However, results differ, dependent on the considered wave. While, for waves 1BT3 and 2BT3, the peak surge motion is smaller in the case of laminar flow, compared to turbulent flow, for wave 3BT2, the peak surge motion is larger in the case of laminar flow, compared to turbulent flow. Also, for the mooring force, larger forces can be observed for the case of laminar flow, compared to turbulent flow, for waves 1BT3 and 2BT3. For wave 3BT3, smaller mooring forces can be found for the case of laminar flow, compared to turbulent flow.

Overall, larger deviations between laminar and turbulent flow conditions can be observed, compared to the findings by Windt et al. (2019a), with an overall maximum difference of 16% in the mooring force for wave 3BT3. From this preliminary study, it is concluded that turbulence has a noticeable effect on the results for the model scale 1:10. Thus, for the subsequent simulations at 1:10 scale, the standard $k-\omega$ SST turbulence model is employed.

It should, however, be noted that the nature of the oscillating flow, and the associated oscillating velocities at the wall of the WEC, make the assessment of the validity of wall functions difficult (Schmitt and Elsässer, 2017). The wall treatment in WSI simulations is still an open research question, and requires future work.

RESULTS & DISCUSSION

In this section, the results for the different WEC geometries, input waves and model scales are presented and discussed. The considered results are the peak heave and surge displacement, pitch angle, and mooring force⁵.

⁴Here, only structure W2 is considered, since it can be assumed that the sharp corners of this structure are more likely to show sensitivity to turbulent effects.

⁵The definition of the peak values follows the CCP-WSI Blind Test Series 3 website (2018)

Table 5 Results for peak heave and surge displacement, pitch angle and mooring force for W2 at 1:10 scale

	Laminar	$k-\omega$ SST	Relative Difference* [%]
1BT3			
Max. heave displ. [†]	0.176m	0.179m	1.7
Max. surge displ.	0.261m	0.297m	12.8
Max. pitch angle	15.933°	13.580°	-2.6
Max. mooring force	11.978N	12.298N	2.6
2BT3			
Max. heave displ.	0.255m	0.255m	0
Max. surge displ.	0.473m	0.502m	5.7
Max. pitch angle	16.047°	14.749°	-8.8
Max. mooring force	17.860N	18.022N	0.9
3BT3			
Max. heave displ.	0.316m	0.313m	-0.9
Max. surge displ.	0.824m	0.805m	-2.3
Max. pitch angle	7.338°	6.315°	-16.2
Max. mooring force	23.832N	23.642N	-0.8

* The relative difference is defined as $k\omega$ SST-Laminar/Laminar

[†] displ. abbreviates displacement

To allow the comparison between the different scales, all results are presented at 1:10 scale, meaning that the results of the 1:1 scale simulations have to be scaled down, using Froude scaling.

Wave maker calibration

Before running the WSI simulations at different scales, the impulse source wave maker must be calibrated to the desired input waves, plotted in Fig. 4. Simulations with a varying source term input, \mathbf{a}_{wm} , are run. Between each simulation, the input is adjusted, according to the difference between amplitude and phase components of the target and resulting wave signal. Details on the calibration methodology are given by Schmitt et al. (2019) and Windt et al. (2019a).

By way of example, Fig. 6 shows the plots of the target and resulting wave for ten subsequent calibration iterations for wave 1BT3. The time traces of the resulting waves 1BT3–3BT3, considered for the final simulations, are plotted in Fig. 7, together with the associated target wave. The numerical waves are chosen based on the minimum root-mean square error between the target and resulting wave, which, in the presented cases, coincides with the minimum deviation at the peak and preceding trough of the focussed wave.

Note that Fig. 7 only shows time traces for 15s, instead of 20s, as in Fig. 6. Since the calibration methodology uses spectral analysis to adjust the wave maker input, longer time traces are beneficial. However, for the submission to the blind test, only the first 15s are of interest.

Wave 1BT3

After the input wave has been calibrated to the desired target wave, the WSI simulations are performed, including structures W1 and W2. Figs. 8 and 11 show the time traces of the heave and surge displacement, the pitch rotation angle and the mooring force, for the case 1:10_{PWT}⁶. In the plots, the red dot marks the peak value, listed in Table 6. Table 6 furthermore contains the results for the 1:1 and 1:10 scale models. In order to determine any underlying difference between the scaled models due to the input wave, the wave-only test case was run at the different scales, and the peak FSE has been extracted. The results listed in Table

⁶Only results for the 1:10_{PWT} are shown here, for brevity. These results are of particular interest, since these are submitted to the Blind Test Series 3.

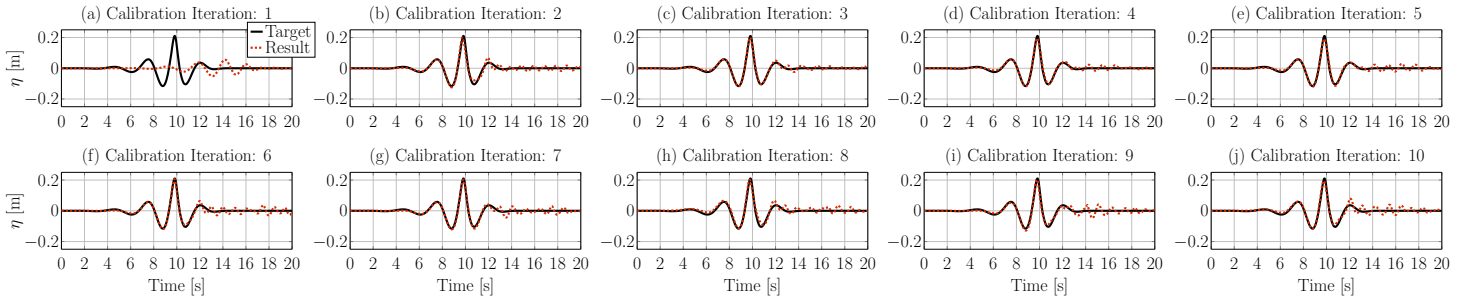


Fig. 6 Target (solid black line) and resulting wave (dashed red line) 1BT3, for ten subsequent calibration iterations.

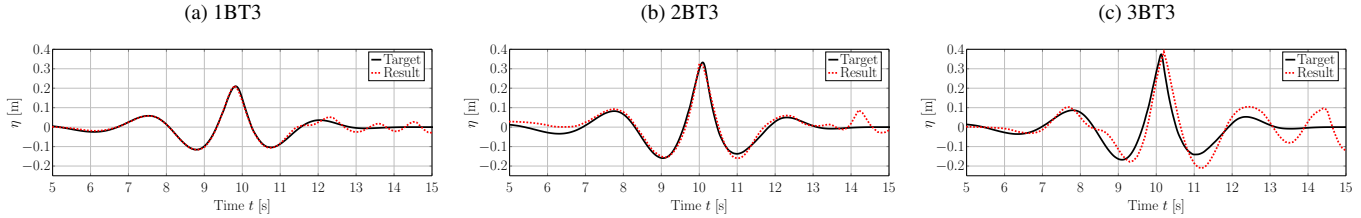


Fig. 7 Target (solid black line) and resulting wave (dashed red line), used in the final WSI simulations.

6 indicate, that negligible differences between the scales occur for the wave-only case.

Table 6 Results for peak heave and surge displacement, pitch angle and mooring force: Wave 1BT3

		1:1	1:10 _{PWT}	1:10
FSE				
Max. η	[m]	0.210	0.213	0.213
W1				
Max. heave displacement	[m]	0.185	0.183	0.186
Max. surge displacement	[m]	0.282	0.269	0.263
Max. pitch angle	[°]	17.561	16.682	16.600
Max. mooring force	[N]	12.553	12.413	12.562
W2				
Max. heave displacement	[m]	0.178	0.178	0.179
Max. surge displacement	[m]	0.268	0.258	0.297
Max. pitch angle	[°]	14.134	14.242	13.580
Max. mooring force	[N]	12.186	12.165	12.297

For the heave motion, relatively small differences between the different scales can be observed. For both geometries, the relative deviation between the results of 1:10_{PWT} and 1:1, as well as 1:10_{PWT} and 1:10 scale, show a magnitude of < 1%. Similarly, relatively small deviations between the mooring forces can be observed for the different scales. The maximum difference, i.e. 1.2%, is found between the 1:10_{PWT} and 1:10 scale model of geometry W1.

Relatively large differences can be found for the surge and pitch motion between the different scales. In surge, the smallest difference of 2.3% is found between the 1:10_{PWT} and 1:10 scale model of W1, and a maximum difference of -15.5% between the 1:10_{PWT} and 1:10 scale model of W2. For the pitch motion, a minimum difference of 0.8% is found between the 1:10_{PWT} and 1:1 scale model of W2, and a maximum difference of -5% between the 1:10_{PWT} and 1:1 scale model of W1.

Wave 2BT3

For wave 2BT3, results for the peak values of the FSE, the translational and rotational motion, as well as the mooring force are listed in Table 7, for W1 and W2 at scale models 1:1, 1:10_{PWT} and 1:10. Figs. 9 and 12 show the according time traces for scale 1:10_{PWT}.

Table 7 Results for peak heave and surge displacement, pitch angle and mooring force: Wave 2BT3

		1:1	1:10 _{PWT}	1:10
FSE				
Max. η	[m]	0.326	0.336	0.336
W1				
Max. heave displacement	[m]	0.266	0.277	0.283
Max. surge displacement	[m]	0.542	0.511	0.436
Max. pitch angle	[°]	22.311	21.603	21.115
Max. mooring force	[N]	18.680	19.121	19.265
W2				
Max. heave displacement	[m]	0.240	0.255	0.255
Max. surge displacement	[m]	0.475	0.464	0.502
Max. pitch angle	[°]	14.955	17.172	14.749
Max. mooring force	[N]	17.010	17.830	18.02

Overall, the differences between the scales show a similar order of magnitude, compared to wave 1BT3, with an overall maximum difference of 14.6% in the surge motion, between the 1:10_{PWT} and 1:10 scale model of W1. For the heave motion, larger differences between the scales can be observed, compared to wave 1BT3, with a maximum difference of 5.9% between the 1:10_{PWT} and 1:1 scale model of W2. Also, for the mooring force, larger differences can be found, compared to wave 1BT3, with a maximum difference of 4.5% between the 1:10_{PWT} and 1:1 scale model of W2. For the pitch motion, the maximum difference is 14.1%, between the 1:10_{PWT} and 1:10 scale model of W2. For wave 1BT3, the difference between these particular scales of W2, is only 4.7%. Overall, a trend towards larger differences between the different scales and WEC geometries can be found, comparing the results of wave 1BT3 and 2BT3. It should, however, be noted that some differences between the

scales 1:10_{PWT} (1:10) and 1:1 may be induced by the difference of the peak FSE (3%), found in the wave-only case.

Wave 3BT3

A similar difference (−5.2%) between the FSE peak values of the 1:10_{PWT} (1:10) and 1:1 scale models can be observed for wave 3BT3. Results for the peak values of the FSE, the translational and rotational motion, as well as the mooring force are listed in Table 8, for WEC geometry W1 and W2 at scale models 1:1, 1:10_{PWT}, 1:10. Figs. 10 and 13 show the according time traces for scale 1:10_{PWT}.

Table 8 Results for peak heave and surge displacement, pitch angle and mooring force: Wave 3BT3

		1:1	1:10 _{PWT}	1:10
FSE				
Max. η	[m]	0.407	0.387	0.387
W1				
Max. heave displacement	[m]	0.343	0.335	0.344
Max. surge displacement	[m]	0.944	0.872	0.800
Max. pitch angle	[°]	39.961	36.852	36.518
Max. mooring force	[N]	25.300	24.320	24.725
W2				
Max. heave displacement	[m]	0.307	0.312	0.313
Max. surge displacement	[m]	0.871	0.817	0.805
Max. pitch angle	[°]	11.410	12.840	9.003
Max. mooring force	[N]	23.794	23.446	23.643

For the heave motion and the mooring force, relatively small differences between the different scales can be found for WEC geometries W1 and W2. For heave, the maximum difference is 1.6%, between scales 1:10_{PWT} and 1:1 of W2. For the mooring force, the maximum difference is −4.0%, between scales 1:10_{PWT} and 1:1 of W1. As for wave 1BT3 and 2BT3, a relatively large difference can be observed for the surge and pitch motion. The overall maximum difference of 30% is found in pitch, between scales 1:10_{PWT} and 1:10 of W2. Given the relatively small errors for the motion in the over degrees of freedom, and the mooring force, it can be assumed that this results is in outlier. In surge, the largest difference, i.e. 8.2%, can be found between scales 1:10_{PWT} and 1:10 of W1.

CONCLUSION

In this paper, an analysis of scaling effects has been carried out on the basis of the case study for the CCP-WSI Blind Test Series 3. To this end, simulations for two WEC structures, at three different scales, have been performed. From the simulations, differences in the order of 10% can be observed between the scales. The results indicate a sensitivity to scaling effects on the considered DoF. For the tested structures, results for the pitch and surge DoF, generally, show larger differences between the scales. However, given the uncertainty regarding the validity of wall function and turbulence modelling, in general, the differences between the scales are considered small.

Future work is required to investigate more precisely the sensitivity of particular DoFs to scaling effects. Furthermore, a detailed analysis of turbulence modelling, including a sensitivity study on the specific turbulence model, at different scales, should be carried out, using experimental data for model validation.

ACKNOWLEDGEMENTS

This paper is based upon work supported by Science Foundation Ireland under Grant No. 13/IA/1886. The research reported in this paper was

furthermore supported by the Higher Education Excellence Program of the Ministry of Human Capacities in the frame of Water science & Disaster Prevention research area of Budapest University of Technology and Economics (BME FIKP-VÍZ).

REFERENCES

- Babarit, A. (2015). A database of capture width ratio of wave energy converters. *Renewable Energy*, 80, 610–628.
- Berberović, E., van Hinsberg, N. P., Jakirlić, S., Roisman, I. V., and Tropea, C. (2009). Drop impact onto a liquid layer of finite thickness: Dynamics of the cavity evolution. *Physical Review E*, 79, 036306–1–036306–15.
- CCP-WSI Blind Test Series 3 website (2018). *Focused wave interactions with floating structures*. accessed 2018-10-12, https://www.ccp-wsi.ac.uk/blind_test_series_3.
- Choi, J. and Yoon, S. B. (2009). Numerical simulations using momentum source wave-maker applied to RANS equation model. *Coastal Engineering*, 56, 1043–1060.
- de O. Falcão, A. F. (2010). Wave energy utilization: A review of the technologies. *Renewable and Sustainable Energy Reviews*, 14, 899–918.
- Elhanafi, A., Macfarlane, G., Fleming, A., and Leong, Z. (2017). Scaling and air compressibility effects on a three-dimensional offshore stationary OWC wave energy converter. *Applied Energy*, 189, 1–20.
- Hirt, C. W. and Nichols, B. D. (1981). Volume of Fluid (VOF) Method for the Dynamics of Free Boundaries. *Journal of Computational Physics*, 39, 201–225.
- Mansard, E. and Funke, E. (1980). The measurement of incident and reflected spectra using a least squares method. In *Proceedings of the International Conference on Coastal Engineering, Sydney*, 154–172. American Society of Civil Engineers (ASCE).
- Menter, F. R. (1992). Improved Two-equation $k\omega$ Turbulence Models for Aerodynamic Flows. Technical report, NASA Technical Memorandum TM-103975.
- Mundon, T. R., Rosenberg, B. J., and van Rij, J. (2017). Reaction body hydrodynamics for a multi-DOF point-absorbing WEC. In *Proceedings of the 12th European Wave and Tidal Energy Conference, Cork*, 997–1–997–10.
- O’Boyle, L., Doherty, K., vant Hoff, J., and Skelton, J. (2015). The value of full scale prototype data-testing Oyster 800 at EMEC, Orkney. In *Proceedings of the 11th European wave and tidal energy conference (EWTEC), Nantes*, 08D–1–1 – 08D–1–11.
- Palm, J., Eskilsson, C., Bergdahl, L., and Bensow, R. (2018). Assessment of scale effects, viscous forces and induced drag on a point-absorbing wave energy converter by CFD simulations. *Journal of Marine Science and Engineering*, 6, 124.
- Schmitt, P. and Elsaesser, B. (2015). A review of wave makers for 3D numerical simulations. In *MARINE 2015 - Computational Methods in Marine Engineering VI, Rome*, 437–446.
- Schmitt, P. and Elsässer, B. (2017). The application of froude scaling to model tests of oscillating wave surge converters. *Ocean Engineering*, 141, 108–115.
- Schmitt, P., Windt, C., Davidson, J., Ringwood, J., and Whittaker, T. (2019). The efficient application of an impulse source wave maker to CFD simulations. *Journal of Marine Science and Engineering*, 7(3).
- Veritas, N. (2000). *Environmental conditions and environmental loads*. Det Norske Veritas.
- Wei, Y., Rafiee, A., and Dias, F. (2013). On the viscous effects in the interaction of water waves with an oscillating wave surge converter. In *Proceedings of the 10th European Wave and Tidal Energy Conference, Aalborg*, 808–1–808–9.

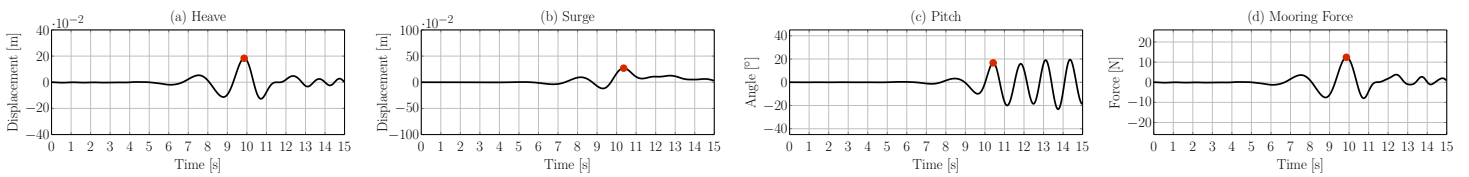


Fig. 8 Motion and force time traces for W1, exposed to wave 1BT3, at 1:10_{PWT} scale

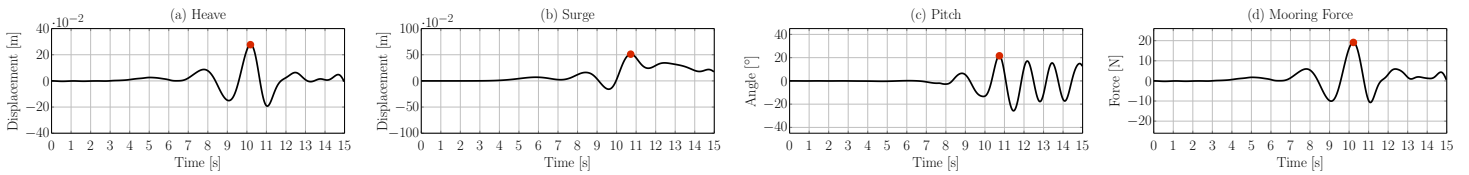


Fig. 9 Motion and force time traces for W1, exposed to wave 2BT3, at 1:10_{PWT} scale

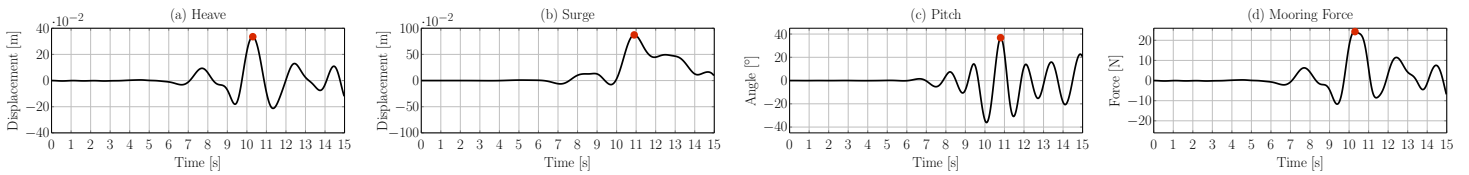


Fig. 10 Motion and force time traces for W1, exposed to wave 3BT3, at 1:10_{PWT} scale

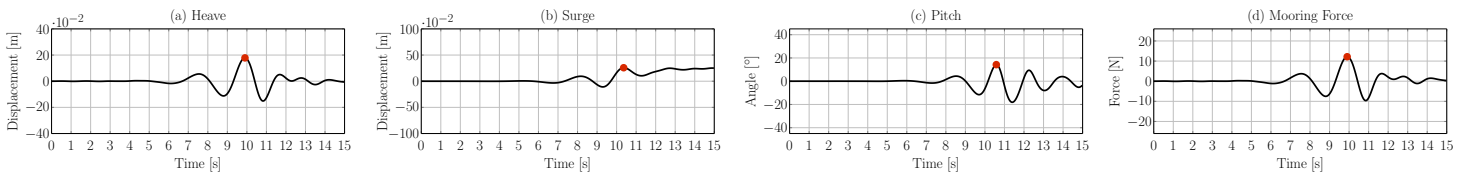


Fig. 11 Motion and force time traces for W2, exposed to wave 1BT3, at 1:10_{PWT} scale

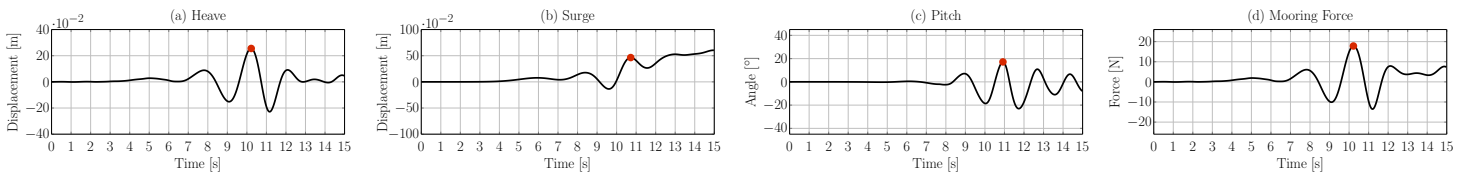


Fig. 12 Motion and force time traces for W2, exposed to wave 2BT3, at 1:10_{PWT} scale

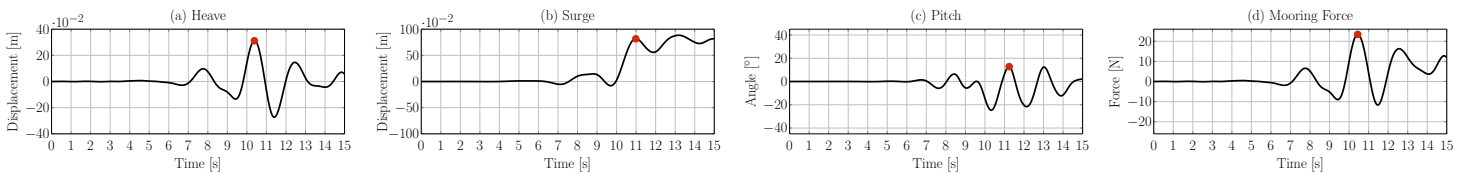


Fig. 13 Motion and force time traces for W2, exposed to wave 3BT3, at 1:10_{PWT} scale

Wei, Y., Rafiee, A., Henry, A., and Dias, F. (2015). Wave interaction with an oscillating wave surge converter, Part I: Viscous effects. *Ocean Engineering*, 104, 185 – 203.

Windt, C., Davidson, J., and Ringwood, J. (2018). High-fidelity numerical modelling of ocean wave energy systems: A review of CFD-based numerical wave tanks. *Renewable and Sustainable Energy Reviews*, 93, 610 – 630.

Windt, C., Davidson, J., Schmitt, P., and Ringwood, J. V. (2019a). Contribution to the ccp-wsi blind test series 2: Cfd-based numerical wave tank experiments employing an impulse source wave maker. *Submitted to the 13th European Wave and Tidal Energy Conference, Naples*.

Windt, C., Davidson, J., Schmitt, P., and Ringwood, J. V. (2019b). On the assessment of numerical wave makers for cfd simulations. *Journal of Marine Science and Engineering*, 7(2).